

Final version, approved for publication in the *Astrophysical Journal*

Measurement of an AGN Central Mass on Centiparsec Scales: Results of Long-Term Optical Monitoring of Arp 102B

Jeffrey A. Newman, Michael Eracleous ¹, Alexei V. Filippenko, and Jules P. Halpern ²

Department of Astronomy, University of California, Berkeley, CA 94720 – 3411

e-mail: jnewman@astro.berkeley.edu, mce@beast.berkeley.edu,

alex@astro.berkeley.edu, jules@jester.berkeley.edu

ABSTRACT

The optical spectrum of the broad-line radio galaxy Arp 102B has been monitored for more than thirteen years to investigate the nature of the source of its broad, double-peaked hydrogen Balmer emission lines. The shape of the lines varied subtly; there was an interval during which the variation in the ratio of the fluxes of the two peaks appeared to be sinusoidal, with a period of 2.16 years and an amplitude of about 16% of the average value. The variable part of the broad H α line is well fit by a model in which a region of excess emission (a quiescent “hot spot”) within an accretion disk (fitted to the non-varying portion of the double-peaked line) completes at least two circular orbits and eventually fades. Fits to spectra from epochs when the hot spot is not present allow determination of the disk inclination, while fits for epochs when it is present provide a measurement of the radius of the hot spot’s orbit. From these data and the period of variation, we find that the mass within the hot spot’s orbit is $2.2_{-0.7}^{+0.2} \times 10^8 M_{\odot}$, within the range of previous estimates of masses of active galactic nuclei. Because this mass is determined at a relatively small distance from the central body, it is extremely difficult to explain without assuming that a supermassive black hole lies within Arp 102B.

Our collection of spectra allows us to apply several tests to models of the source of the double peaks. The ratio of H α to H β flux at a given velocity displays no turning points or points of inflection at the velocity associated with the blue peak in flux; thus, this peak should not correspond to a turning point in physical conditions. This

¹Hubble Fellow

²Permanent Address: Department of Astronomy, Columbia University, 538 West 120th Street, New York, NY 10027, e-mail: jules@carmen.phys.columbia.edu

behavior is consistent with simple accretion disk and, possibly, spiral shock models, but not with models which attribute the double peaks to separate broad-line regions around a binary black hole or to broad, subrelativistic jets. The lack of systematic change in the velocity of the blue peak over time provides a further constraint on binary broad-line region models; this yields a lower limit on the mass of such a binary black hole system of at least $10^{10} M_{\odot}$. The variability properties of the double-peaked emission lines in Arp 102B therefore continue to favor an accretion disk origin over other models.

Subject headings: accretion, accretion disks – galaxies: active – galaxies: nuclei – galaxies: individual (Arp 102B) – line: profiles

1. Introduction

Although there is a broad consensus that disk accretion onto a supermassive black hole provides the tremendous power of active galactic nuclei (AGNs), direct evidence for that process has remained elusive. The accretion disks expected from theoretical models are too compact to resolve in even the nearest galaxies, and any optical emission lines that would display the dynamical signature of the disk are evidently too faint to be detected easily, at least in most cases. There does, however, exist a class of AGNs (the “double-peaked emitters”) whose spectra exhibit hydrogen Balmer emission lines having two broad peaks (one redshifted and one blueshifted) widely separated from the systemic velocity of their host galaxy (Eracleous & Halpern 1994). In many other cases, such as the H I spectra of spiral galaxies and the optical spectra of cataclysmic variables (Marsh 1988; Young & Schneider 1980), this kind of line profile is the spectroscopic “signature” of gas rotating in a disk. One of the first AGNs in this class to be so identified was Arp 102B, a broad-line radio galaxy at a redshift of 0.02437 (Halpern & Filippenko 1988). Models of either circular or elliptical photoionized accretion disks typically give good fits to the Balmer line profiles of this and other, similar objects. Furthermore, an accretion disk provides the most straightforward interpretation of the absence of double-peaked components in high-ionization broad lines (Halpern *et al.* 1996).

Alternative models that may produce double-peaked emission lines have been proposed. A binary black hole with broad line emission peaking around each member (Gaskell 1983), a wide (in opening angle) subrelativistic bipolar outflow (Zheng, Binette, & Sulentic 1990), or emission from spiral shock waves within a disk (Chakrabarti & Wiita 1994) may all produce spectra with multiple peaks displaced from the systemic velocity.

Changes in the emission-line profiles over time may allow discrimination among these models. For instance, in the binary broad-line region (BLR) model, the two peaks should behave as a double-lined spectroscopic binary; determination of the period and velocity amplitude of this variation would constrain the combined mass of the central objects.

If a disk origin for the emission lines were established, the patterns and time scales of variability might provide information about the structure and behavior of disks. The line profiles of elliptical disks will change their shape in a characteristic way as the disk precesses (Eracleous *et al.* 1995), while other variations may indicate the presence of inhomogeneities in the disk. Simple spiral shock models sometimes produce a third peak at lower velocity and predict patterns of evolution of the line profile (Chakrabarti & Wiita 1993, 1994). Detected reverberation might constrain all models, since it could specify the length scales involved. More detailed reverberation observations could provide even stronger limits on models of the structure of the BLR (Blandford & McKee 1982; Stella 1990).

One feature of the spectrum of a circular accretion disk is that the blue peak is brighter than the red one due to relativistic boosting (in this paper, “blue peak” refers to the peak with smaller wavelength). Miller & Peterson (1990) have asserted that, since one Lick image dissector scanner (IDS; *cf.* Robinson & Wampler 1972) spectrum of Arp 102B appeared to have a higher red peak than blue, the accretion disk hypothesis is excluded. However, as will be shown below, a simple non-axisymmetric disk model can easily reproduce such profiles. We note that none of our spectra, including ones taken roughly two months before and a year after theirs, contains such a strong, rounded feature in the Balmer lines. Furthermore, our spectra with narrow lines removed appear to peak at a substantially different wavelength from the peak found by Miller & Peterson (an average of about 6695 Å versus roughly 6650 Å respectively). It is possible that they in fact observed a particularly intense but very short-lived “hot spot” of the sort described in §4.2, below.

Motivated by the possibility of testing the accretion disk and other models, we have monitored the behavior of the optical emission-line spectrum of Arp 102B from 1983 through the present. Consecutive observations were separated by intervals as short as a day and as long as two years. This paper presents the results of that campaign through June 1996. We model the double-peaked profile of H α as emission from an accretion disk, in addition to evaluating the applicability of the other models described above. Our models of the variation of the line profile produce a determination of the mass of the central object directly from its gravitational effects on scales of less than a centiparsec. We describe the observations in § 2 and the measurements made using the data in § 3, apply accretion disk models in § 4, examine the implications for other models in § 5, and discuss the results in § 6.

2. Observations

We have been observing the optical spectrum of Arp 102B since 1983 using several telescopes, as listed in Table 1. Some of these spectra have been published previously (Halpern & Filippenko 1988, 1992; Eracleous & Halpern 1993).

The spectra of double-peaked emitters generally include appreciable contributions from starlight as well as a substantial nonstellar continuum component. These were removed from

the data by subtracting a linear combination of normalized spectra of template galaxies (from a previously collected library of spectra of E and S0 galaxies) and a power law. For the continuum around $H\alpha$, spectra of NGC 7332 and UGC 555 provided the best fit out of the library galaxies. For the continuum around $H\beta$, other template galaxies had to be used as those spectra which fit best around $H\alpha$ did not extend to the shorter wavelengths. For both spectra around $H\alpha$ and around $H\beta$, subtracting the best fitting combination of templates and power-law resulted in a flat residual very close to zero flux. Strong stellar absorption features such as Na I D were largely removed, and narrow He I $\lambda 5876$ was typically visible in emission.

The fluxes of the starlight- and continuum- subtracted spectra were normalized using the integrated flux in narrow [O III] $\lambda 5007$ (for spectra around $H\beta$) or narrow [O I] $\lambda 6300$ (for spectra around $H\alpha$). Since the narrow-line region of Arp 102B is marginally resolved, variations in observing conditions and extraction width among the observations yield different relative amounts of the narrow- and broad- line fluxes included in the spectra; thus, these normalizations are only approximate. In this paper, no results depend upon the absolute normalizations of the spectra, as we interpret only the changes in the shape of the line.

3. Data Analysis

3.1. Relative Flux in the Two Peaks

It has been clear since the work of Halpern & Filippenko (1988) that the shape of the Balmer lines of Arp 102B varies significantly. One way to parameterize the evolution of the line profile is to measure the relative fluxes of the blue and red peaks. To estimate this, the average flux between 6400 and 6520 Å (in the rest frame of the AGN) was used to measure the flux in the blue peak, while the average flux in the combined ranges 6600 – 6700 and 6760 – 6780 Å was associated with the flux in the red peak. These wavelength ranges were selected to avoid all of the major narrow emission lines and the range that the “standard” BLR (in $H\alpha$) would occupy (*cf.* Halpern *et al.* 1996). Significantly altering these ranges changed the average flux by less than 1.5% of the original value in each case; thus, this method effectively measures changes in the ratio of the *average* fluxes in the two peaks.

To address the question of whether the maximum flux on the blue peak exceeds that on the red peak in any spectrum, we would like to measure the ratio of those quantities. The [S II] lines prevent any precise measurement of the flux at the top of the red peak, however. To estimate the ratio of the maximum fluxes of the two peaks, the average flux ratio, measured as described above, was multiplied by a constant determined using a previously published model fitted to one spectrum of Arp 102B (Eracleous & Halpern 1994) to approximate the actual shape of the red peak of that spectrum (no physical significance of that model is assumed at this stage). Multiplication by this constant does not necessarily yield the actual ratio of the peak fluxes for each epoch. However, the conclusions of this paper will not be affected if the red-to-blue ratio

(which, with this normalization, we will refer to as R) is multiplied by any factor.

Figure 1 shows the history of the ratio R , determined using the method described above. At some epochs, R approaches or may even exceed unity, though the spectrum with the most extreme value of R is of lower quality than most (likely due to being the first following a spectrograph replacement at Lick Observatory). It is very difficult to prove that the red peak in fact has the greater flux due to the confusion of the narrow lines with that peak. Nevertheless, it would appear that the behavior of the $H\alpha$ profile of Arp 102B cannot be completely explained by any *axisymmetric* disk model. It is striking that there is an interval during which R appears to vary sinusoidally with an amplitude of about 16% of the average value; the variation begins in 1991 and seems to decrease in amplitude during 1995. Figure 1 presents a fit to those points designated with error bars; the error bars shown are based upon the uncertainties in determining the red and blue fluxes as described above. The dashed line indicates the fitted curve

$$R = R_0 + R_1 \cos \left[\frac{2\pi}{P}(t - t_0) \right], \quad (1)$$

where R is the red-to-blue flux ratio, P is the period of variation, and t is the Julian date, with $R_0 = 0.8637 \pm 0.0087$, $R_1 = 0.1371 \pm 0.0099$, $P = 790 \pm 25$ days, and $t_0 = 2449634 \pm 23$ days. Compensating for cosmological time dilation, the period in the rest frame of Arp 102B is $P/(1+z)$, or 771 ± 24 days. This sort of variation may not be unique to Arp 102B; Veilleux & Zheng (1991) have reported similar, albeit slower, variations in the ratio of the fluxes of the two peaks of the $H\beta$ line of 3C 390.3. However, no more than one cycle of that period was observed in 3C 390.3, and later data do not confirm it (Gilbert *et al.* 1997). A similar variability pattern is also observed in 3C 332 (Eracleous 1997). Possible implications of this variation of Arp 102B will be discussed in § 4.2.

3.2. The Velocity of the Blue Peak

The binary BLR model predicts that the two peaks should exchange their positions relative to the rest wavelength with a period dependent upon their combined mass, as in a double-lined spectroscopic binary. The expected period could be a few decades if the combined mass of the binary is $\sim 10^8 M_\odot$. We therefore measured the position of the blue peak in our spectra of Arp 102B in search of the velocity variations that this hypothesis predicts. We have used Pogson’s method (see Gaskell 1996, and references therein) and fits to the peak with Gaussian and quadratic functions for such measurements. Pogson’s method yields results that are sensitive to substructure and skewness in the peak, while Gaussian fits give a rough flux-weighted centroid of the line. The two methods are compared in detail and discussed in a separate paper devoted to testing the binary black-hole hypothesis in a number of double-peaked emitters (Eracleous *et al.* 1997).

The results obtained using Pogson’s method and the Gaussian fitting method are given in Table 2. In Figure 2a we present these results graphically by plotting the measured peak velocity

(determined from the wavelength relative to that of the narrow $H\alpha$ line using the standard relativistic formula) as a function of time. Uncertainties in these measurements are typically of order 1 \AA , which translate into uncertainties in the velocity of the peak of less than 100 km s^{-1} . However, systematic effects dominate the uncertainty in the location of the peak. In particular, the detailed shape of the profile around the peak varies on time scales shorter than a year. In the binary BLR model, these variations could be attributed either to reverberation of the individual BLRs in response to a varying ionizing continuum or to changes in the distribution and/or velocity field of the line emitting gas. To bypass these uncertainties, we have computed annual averages of the peak locations and have taken the root-mean-square dispersion of the velocities for a given year to be the uncertainty of their average. Our own data were supplemented by a measurement based on the spectrum of Stauffer, Schild, & Keel (1983) as reported in Halpern & Filippenko (1988).

3.3. The $H\alpha$ to $H\beta$ Flux Ratio

Although most of our spectra include only a wavelength range around $H\alpha$, a smaller number include $H\beta$ as well. The ratio of the $H\alpha$ to $H\beta$ flux at a given velocity (hereafter H) provides an indication of the physical conditions, particularly the ionization parameter and to a lesser extent the temperature and the density, of the emitting gas at that velocity. It therefore may constrain possible models for the source of the Balmer line emission.

Figure 3 shows H for those years with enough spectra that included $H\beta$ to allow significant reduction in noise through averaging. The value of H appears to vary monotonically across the entire blue peak. Though largely obscured by the presence of narrow emission lines near either $H\alpha$ or $H\beta$, the behavior on the red peak appears to also be consistent with a turning point at zero velocity only. Since there are no points of inflection or turning points in H at the velocity of the blue peak, it would seem that physical conditions in the emitting material do not have a turning point at that velocity.

This is precisely the behavior we would expect if an accretion disk emits the double-peaked Balmer lines. In that model, the locations of the peaks correspond to the velocities with the greatest integrated flux from the entire disk, not to a special region (such as the inner or outer edge). If the two peaks are produced by gas around each of the black holes of a binary system, in contrast, one might expect H to have a turning point where the $H\alpha$ flux reaches a peak, since that presumably occurs at the velocity of one of the black holes; admittedly, this scenario has not been modeled in detail. One would also expect a turning point in H at the flux maximum in a model where the two peaks correspond to broad jets, since the peak flux should correspond to the most emissive parts of a jet. The behavior of H within the spiral shocks model of Chakrabarti & Wiita (1994) is less clear.

4. Application of Accretion Disk Models

4.1. Circular and Elliptical Disks

The variation of the two peaks that began in 1990 provides an additional means of testing accretion disk models. The difference between an observed spectrum and a well-fitting model for disk-like emission would be expected to include the narrow lines present and, potentially, a broader component about $H\alpha$ resembling that of typical BLRs. The presence of a broad $H\alpha$ line from Arp 102B originating in a region which is physically distinct from the source of the double-peaked lines is an almost inescapable conclusion from the ultraviolet line spectrum (Halpern *et al.* 1996). We might also expect our model fits to underestimate flux at the edges of the line profile, since Gaussian broadening and a step-like decrease to zero of the disk’s emissivity as a function of radius are assumed to approximate the combined effects of Compton scattering, turbulence, and physical conditions that presumably vary more smoothly across the disk. In this paper, we demanded a closer fit of data to the models than in existing published work.

In previous papers, models of circular, axisymmetric accretion disks provided adequate fits to the presented spectra of Arp 102B (Chen, Halpern, & Filippenko 1989; Chen & Halpern 1989). However, as might be expected from the discussion of the previous section, such models cannot provide a good fit to the profile from late 1990 through 1995. An axisymmetric disk model did provide an excellent fit to the spectrum of 1990 July 17, the last spectrum of good quality before the sinusoidal variation in R began. The parameters of that fit were: power law index of the variation of emissivity with radius $q = 3.0$; line broadening given by convolution with a Gaussian with standard deviation $b = 1050 \text{ km s}^{-1}$; disk inclination $i = 30.8^\circ \pm 1^\circ$, and inner and outer disk radii $\xi_i = 305$ and $\xi_o = 730$ gravitational radii (the gravitational radius $r_g = GM/c^2 = 1.4745 \times 10^{13} M_8 \text{ cm}$, where G is Newton’s gravitational constant, M is the mass of the presumed central body, c is the speed of light, and M_8 is the mass of the central body in units of $10^8 M_\odot$). These values were used as a basis for the circular disk portion of the models described below. Of these parameters, only the inner and outer radii of the disk were allowed to vary in later models (*q.v.*, below).

Following the inadequacy of the circular disk models, we attempted to fit representative spectra that had extreme values R with the elliptical disk models of Eracleous *et al.* (1995). These models provided an excellent fit to those spectra with R well below unity. However, much poorer fits to those spectra with excess red flux were achieved, and only then by allowing the eccentricity to vary from 0.1 to 0.59, the power law index q to vary from 2.2 to 3, and i to vary from 28° to 31.5° , all simultaneously. Such variations are more or less unrealistic. For instance, Syer & Clarke (1992) have demonstrated that the eccentricity of an accretion disk should change only slowly except in its innermost portions. Inspection of their figures and the estimates of Eracleous *et al.* (1995) indicate that circularization by general relativistic precession is effective only within about 100 gravitational radii, while viscous circularization acts only over the very long viscous time scale. That, along with the fact that even with seven free parameters only marginally satisfactory

fits could be produced with $R \approx 1$, would seem to indicate that the variations observed among the spectra are not due to, for instance, a precessing elliptical disk.

4.2. Circular Accretion Disk with a Hot Spot

Eracleous *et al.* (1995) described the basic models of circular and elliptical accretion disks adapted here; the original circular disk models are described in Chen, Halpern, & Filippenko (1989) and Chen & Halpern (1989). The only significant addition to the previous algorithm here is the inclusion of a region of the disk with excess emissivity (hereafter called a “hot spot”). Line-emitting hot spots at the intersection of a disk with an accretion stream have been observed in the disks around cataclysmic variables (Marsh *et al.* 1990), and a number of phenomena might produce them in an AGN accretion disk. In fact, a hot spot model for variation in the emission-line profile of 3C 390.3 has been proposed by Zheng, Veilleux, & Grandi (1991).

We assume for our model the presence of a circular, rather than elliptical, accretion disk to minimize the number of free parameters. The hot spot is then implemented as an excess of emissivity within the disk along a circular arc of infinitesimal extent in radius. The local viscous time scale, which is the time scale over which any sort of instability may propagate radially, is larger than the period of an orbit for radial extents of the instability above about $3 \times 10^{10} \alpha M_8^2 T_4$ cm at radii of interest, where α is the traditional Shakura & Sunyaev (1973) viscosity parameter and T_4 is the temperature of the disk in units of 10^4 K, applying the definitions of time scales used below (*cf.* equations 3 and 9). Thus, even if the disturbance is not infinitesimal in radial extent, its radial evolution should not be significant. The excess emissivity of the hot spot is assumed to vary as a Gaussian in azimuthal angle along its arc away from the center of the hot spot.

Thus, the model requires four additional parameters (beyond those in a circular disc model). The first is ξ , the distance from the hot spot to the central body in terms of the gravitational radius. The second parameter is θ , the azimuthal angular position of the hot spot’s center measured within the disk. When $\theta = 270^\circ$, the hot spot has its greatest velocity towards the Earth. The remaining parameters are σ , the standard deviation of the Gaussian dependence of emissivity on angle away from the hot spot’s center, in degrees; and I , a normalization factor representing the ratio of the hot spot’s maximum (*i.e.*, central) emissivity to that of the disc at the same radius. Thus, the rest frame luminosity of a hot spot relative to the disk luminosity is

$$\frac{L_{spot}}{L_{disk}} = \frac{\int_0^\infty \int_0^{2\pi} I \xi^{-q} e^{-\frac{(\theta - \theta_{spot})^2}{2\sigma^2}} \delta(\xi - \xi_{spot}) \xi d\theta d\xi}{\int_{\xi_i}^{\xi_o} \int_0^{2\pi} \xi^{-q} \xi d\theta d\xi} = \frac{\sigma I}{\sqrt{2\pi}(\xi_o - \xi_i)} \frac{\xi_i \xi_o}{\xi_{spot}^2}, \quad (2)$$

where I , θ_{spot} , σ , and ξ_{spot} are the hot spot parameters described above (with σ here given in radians), and both $q = 3$ and $\sigma \ll 2\pi$ were assumed in evaluating the integrals.

In contrast to models with only a simple accretion disk, models of a circular accretion disk with a hot spot provided an excellent fit to all of the spectra during the time of variation in R .

We varied as few parameters as possible in the course of the fits; excellent fits were found for all spectra while varying only five parameters among them. The first of these are ξ_i and ξ_o , the inner and outer radii of the axisymmetric disk, which may be expected to vary substantially because of changes in the ionization structure of the disk (which determines the location of Balmer-line emission). The ionization state within the disk will respond to the amount of ionizing flux very quickly (the recombination time scale in such a disk is expected to be on the order of minutes, substantially less than the light-crossing time). That ionizing flux is presumably determined by variability in the innermost parts of the disk, and thus would also be expected to vary over much shorter periods than the time for light to travel from the inner to the outer edge of the disk. Thus, the inner and outer radii of the Balmer-emitting disk should not be expected to vary in concert, but instead with relative (though short) delays.

Similarly, we allowed the normalization of the hot spot flux, I , and the standard deviation of its flux decline in angle, σ , to vary. Neither is determined by the fitting process to better than perhaps 30%. We note that σ varies over a substantial range among all the models, and the hot spot intensity parameter I decreases substantially after 1994. Finally, θ , the azimuthal angle of the hot spot along its orbit about the disk, has to vary over 360° to be able to complete multiple cycles of enhancing at some times the red peak and at others the blue. Table 3 presents the results of these fits. Note that in all cases, the hot spot represented a perturbation of only a few percent in the total Balmer line flux of the disk. Due to the ambiguity of the helicity of the hot spot’s orbit from what are effectively radial velocity measurements, there are two possible values of θ for each model fit; only one is listed in the table. Figures 4 and 5 display representative model fits. Even in 1995, when the variation in R is no longer sinusoidal, the spectra are better fitted by a model with some hot spot component (though with a lower normalization than before) than by an axisymmetric disk. Thus, it appears that the hot spot gradually decreases in strength.

In all model fits plotted in this paper the hot spot was kept at a radius ξ of 455. This radius was chosen based upon fits to data in the interval 1991 June 17 – 20, when the azimuth of the hot spot was near 270° , so that its wavelength was shortest (and thus furthest from the interference of narrow lines). In fact, a good fit to that spectrum was possible for models with ξ from 355 to 485, but beyond those bounds the fits were noticeably worse.

That models with a single hot spot radius fit all of the spectra is not in and of itself convincing; it is conceivable that some other phenomenon might produce similar behavior. However, if we adopt the hot spot model, we know from Kepler’s laws how a body must travel in a symmetric potential along a circular orbit; in particular, it must move with constant angular velocity in such a case. Figure 6 plots the possible value of θ nearer the line corresponding to the phase of the sinusoidal variation in R (taking the solution with positive angular velocity) for each of the modeled spectra versus the date of observation of that spectrum. The depicted error bars of $\pm 30^\circ$ are a crude estimate based upon the modeling.

It might be contended that the line fits so well so often simply by virtue of having two possible

points to fit at any given date (note that only the possible θ which better fits the phase curve of positive angular velocity is plotted). However, if points are distributed randomly, there is only a 1 in 3 chance that the line will be within 30 degrees of either point for a given epoch. Clearly, more than the expected 7 points (namely, 14) are within their error bars of the line; the probability of this many or more points falling so close by chance is only 0.18%. We also note that residuals about the fit line do not appear to occur systematically for a given phase at different epochs; thus, the motion seems strongly consistent with constant angular velocity.

We have determined the period of what seems to be an orbital motion through the evolution of R (or, alternatively, through the evolution of θ in the models). Indeed, the only proposed sources of variability in an AGN that would cause simple sinusoidal variation in R with little apparent decay (in amplitude or frequency) for nearly two complete cycles are orbital in nature. We have also determined, through our models, the radius ξ (in terms of the gravitational radius, r_g , which is proportional to the mass) associated with that motion. There are no ambiguities in the orbital inclination so long as the “hot spot” is presumed to lie within the disk, which seems very likely. These data are, then, sufficient to find the mass within the orbit of the hot spot (assuming a spherically symmetric mass distribution) by the complete form of Kepler’s third law for a circular orbit:

$$P = 2\pi\sqrt{\frac{r^3}{GM}} = \frac{2\pi GM\xi^{3/2}}{c^3}, \quad (3)$$

where P is the period of the orbit and $r = \xi r_g$ is its radius.

Using the above values for the period and radius of the hot spot, we find $M = 2.21_{-0.73}^{+0.23} \times 10^8 M_\odot$, within the range of previous estimates of masses of AGNs. For this mass and $\xi = 455$, the physical radius of the hot spot’s orbit is 4.80×10^{-3} pc. This corresponds to an average density for a sphere with the same radius as the orbit of $2.38 \times 10^{14} M_\odot \text{pc}^{-3}$. Such a density is extremely difficult to accomplish without the presence of a supermassive black hole.

5. Evaluation of Alternative Models

5.1. Binary Black Holes

We may expect the orbit of any binary black hole system to be circular, as it should have evolved to its present state through dynamical friction. If we adopt an analogy between a binary black hole system and a stellar, double-lined spectroscopic binary, the velocities of the two peaks should vary sinusoidally. Accordingly, we have fitted the velocity variations of the blue peak with a curve of the form

$$v_{\text{obs}}(t) = v \sin i \cos \left[\frac{2\pi}{P_{\text{orb}}} (t - t_0) \right], \quad (4)$$

where $v_{\text{obs}}(t)$ is the observed radial velocity of the blue peak as a function of time, v is the orbital velocity of the corresponding black hole, i is the inclination of the orbital plane of the binary, t_0 determines the phase of the orbit, and P_{orb} is the orbital period. The fitting algorithm used, which is described by Eracleous *et al.* (1997), determines the confidence intervals of the model parameters in addition to the best fit.

In Figure 2b we show the variation of the annually averaged velocity of the blue peak of the H α line of Arp 102B between 1982 and 1996 using measurements made with the Gaussian fitting method. The dashed line in this figure is the best fitting sinusoidal velocity curve, which corresponds to a period of 390 years and an amplitude of 5200 km s $^{-1}$. The fit is quite poor, and the scatter of the data points about the best-fitting curve does not seem random. We find that a sinusoidal modulation of the velocity of the blue peak must have a period greater than 114 years to be even marginally consistent with the data. If the data from 1990 and 1991, when the centroid of the blue peak seems to be varying rapidly, are excluded, the lower limit to the period (and hence the mass) increases by a factor of 2.

The above observational constraints place a lower limit on the total (combined) mass of the two black holes required by the binary BLR model. We note that the blue peak has a smaller velocity displacement from the rest wavelength of the line than the red peak, which associates it with the more massive of the two members of the hypothesized binary. Under this condition we can customize Kepler’s third law to produce an expression for the lower limit on the mass of the binary (*cf.* Eracleous *et al.* 1997),

$$M > 4.7 \times 10^8 (1 + Q)^3 \left(\frac{P_{\text{orb}}}{100 \text{ yr}} \right) \left(\frac{v \sin i}{5000 \text{ km s}^{-1}} \right)^3 M_{\odot}, \quad (5)$$

where Q is the mass ratio of the binary, estimated to be about 1.5 from the relative velocities of the two peaks.

The observational constraints derived above using all of the data yield a lower limit to the total mass of $10^{10} M_{\odot}$. This is the lowest limit that the data will admit, and it is not reduced if measurements made with Pogson’s method are used. This bound is rather restrictive, since it is a significant fraction of the mass of an entire galaxy, making the binary black hole hypothesis unlikely for Arp 102B. We stress that we are only able to constrain the specific scenario in which each of the two peaks of the line originate in gas surrounding one of the two black holes. In this context, the velocities of the two peaks require that the mass ratio of the two black holes be of order unity. One can envisage alternative scenarios that are not constrained by the data we have presented here. For example, the nucleus may harbor a supermassive binary in which one black hole is significantly more massive than the other and accretes at a much higher rate. In such a scenario, an accretion disk around the more massive black hole can be the source of the double-peaked line, but the location of the twin peaks varies slightly as a result of the perturbation from the companion.

5.2. Jets and Outflows

Jets such as those proposed to produce double-peaked Balmer emission lines must be quite different from those previously observed in AGNs. If continuous flows, these jets have to be subrelativistic to produce peaks at the correct wavelengths and have very broad opening angles to produce substantial flux at zero velocity (*cf.* the models of Zheng, Veilleux, & Grandi 1990), but still have sufficiently low velocity gradients to produce substantial optical depth; this is a strong constraint (Halpern *et al.* 1996). Alternatively, the jet emission might occur at the intersection of a rapid jet and an extremely turbulent (with velocity width $\approx 1000 \text{ km s}^{-1}$), massive cloud. However, it is unclear why such a phenomenon might produce two widely displaced peaks more commonly than one.

Although radial outflow models as a class are very difficult to constrain, specific versions of such models may be tested observationally. In particular, Livio & Pringle (1996) have pointed out that an accretion disk, if present, will obscure the receding parts of an outflow at small radii from its center. This suggests that if double-peaked lines are to be attributed to an outflow, they must originate in parts of that outflow far enough from the center of the disk not to be obscured. Moreover, if a central source of ionizing radiation powers the line emission from the outflow, variations in the luminosity of the source will result in corresponding changes in the flux of the line. The difference in light travel time between the two sides of the outflow and an observer on the Earth dictates that the two sides of a double-peaked emission line should not respond simultaneously, but rather with a delay of order $0.7 M_8 \text{ yr}$. In this scenario, with the assumption that the flow accelerates along the jet, the profile variations should have a very specific pattern: a change should appear at low velocities first and then propagate towards high velocities. This type of perturbation should first appear on the blue side of the line profile, and then its mirror image on the red side should follow with a delay as estimated above. In contrast, the seemingly orbiting source of emission we observe in Arp 102B (*cf.* §4.2) first appears on the red side of the line and moves from one side of the line to the other. Any identification of this variable emission with a phenomenon propagating along both jets would demand considerable fine-tuning of time delays between the two peaks and other physical conditions. The variable part of the emission not only passes from one side of the peak to the other but also returns to its original peak at the correct time, requiring some sort of repeated phenomenon in the jet with its period closely matching the time delay between the peaks.

5.3. Spiral Shocks in a Disk

Spiral shock models cannot easily accommodate the time scale of Arp 102B's periodic variation. Though such models do predict variations in the line profile that pass from one side of the rest wavelength to the other, the period of such variations will be roughly the viscous time scale. For one-armed spiral waves (which the dispersion relation strongly favors over higher order

displacements), Kato (1983) calculates a period

$$\tau = \frac{2\pi\Omega_K r^2}{c_s^2 w_*} = \frac{6.6 \times 10^4 \xi^{1/2}}{T_4 w_*} \text{ yr}, \quad (6)$$

where r is the radius at which the time scale is defined, Ω_K is the angular frequency of a Keplerian orbit at that radius, c_s is the sound speed, and w_* is a parameter believed to be less than one (equal to the viscosity parameter α in the Shakura-Sunyaev model for a period of $2\pi t_{visc}$). Since ξ is at least 3 for stable orbits about a compact body, this is clearly much longer than the observed period of variation. Furthermore, previously described spiral shock models generally include a third, minor peak at some epochs, and the two major peaks are expected to also move about in wavelength on the pattern time scale; these do not fit the variations seen.

It is also conceivable that a corrugation wave, which causes a periodic warping of the disk, might produce similar variations (Kato 1989). Such a wave travels around the disk on roughly the sound-crossing time,

$$\tau_{cross} \approx \frac{80 M_8 \xi_2}{T_4^{1/2}} \text{ yr}, \quad (7)$$

where ξ_2 is ξ in units of 10^2 ; this can match the observed time scales only for masses around $10^6 M_\odot$. A warp can also be produced in the disk by an irradiation-induced instability, described by Pringle (1996). The precession time scale of the warp is given by (following Storchi-Bergmann *et al.* 1997)

$$\tau_{prec} \approx 7 \times 10^5 \left(\frac{m_{disk}}{10 M_\odot} \right) \frac{M_8^{1/2}}{\xi_2^{1/2} L_{43}} \text{ yr}, \quad (8)$$

where m_{disk} is the mass of the accretion disk (estimated to be of order $10 M_\odot$) and L_{43} is the X-ray luminosity in units of $10^{43} \text{ erg cm}^{-2} \text{ s}^{-1}$. Both of the above time scales are too long to account for the observed profile variability in Arp 102B. Moreover, Pringle (1996) estimates that the radiation-driven instability would operate at radii of order 0.1 pc, much larger than the scales we are interested in here.

6. Discussion and Conclusions

A model attributing the variability of the broad, double-peaked $H\alpha$ profile of Arp 102B to a hot spot on a circular orbit is consistent with several tests of the data over more than two complete cycles in the red-to-blue flux ratio variations of the peaks. Both the modeling described here and other observations of Arp 102B (e.g., Halpern *et al.* 1996) agree with the hypothesis that the remaining emission is due to a circular accretion disk. It seems clear from the discussion of the preceding section that the variable excess emission is not associated with subrelativistic jets or spiral shock waves. If such structures were indeed present, a separate origin for the periodically varying part of the line would have to be invoked. In that case, the variable part of the line would still be emitted at a radius within the range expected for the Balmer-line emitting part of

an accretion disk. In such situations, however, our mass determination would have an additional uncertainty, since the inclination of the orbit of the source of the variable emission would no longer be known.

If some materially coherent, orbiting source of emission did not lie within a circular accretion disk, it is likely to have a substantially elliptical orbit (as there are few strong circularizing effects operating on time scales of a few years). However, in such a case, fitting the excess emission by assuming a hot spot along a circular orbit should require substantially varying angular velocity (*i.e.*, the slope of the angle vs. time curve), in contrast to what is observed. Thus, the assumption that the double peaks of Arp 102B are produced by a circular accretion disk yields a natural explanation for the constant angular velocity of a region of excess emission; this provides further support for the accretion disk hypothesis.

The fact that the hot spot persists with roughly constant strength through two orbits and then decays over a shorter time scale allows some evaluation of the possible source of that excess emission. If it dissipates due to viscous processes, for instance, it must be extremely compact compared to the disk as a whole, since the viscous time is

$$\tau_{visc} = \frac{l}{v_R} \approx \frac{48.2}{\xi^{1/2} M_8 \alpha T_4} \left(\frac{l}{R_\odot} \right) \text{ yr}, \quad (9)$$

where l is the characteristic radial size of the disturbance and v_R is the radial velocity of gas within the disk relative to its center.

Disturbances can propagate azimuthally (through 360°) or vertically (through one scale height) on the Keplerian orbit period; from the behavior of R , we may conclude that this is roughly 2.2 years, somewhat longer than the period over which the damping occurs. The hot spot may dissipate thermally over the time scale

$$\tau_{th} \approx \frac{\theta}{\Omega_K \alpha} \approx \frac{0.1 M_8 \xi_2^{3/2} \theta}{\alpha} \text{ yr}, \quad (10)$$

where θ is the azimuthal angular extent of the hot spot. The hot spot appears to decrease in intensity over an appreciable fraction of a year; thus, for this mechanism to operate, it should have substantial azimuthal extent or α should be much less than unity. Heat waves will propagate in the time it takes sound to travel along the spot,

$$\tau_{sound} \approx \frac{80 M_8 \xi_2 \theta}{T_4^{1/2}} \text{ yr}, \quad (11)$$

requiring a very small angular extent (which, based upon the values of σ providing best fits, is almost certainly less than 20°) or a high internal temperature for the hot spot to dissipate its energy.

One constraint on the radial structure of the hot spot may be found from its azimuthal evolution, since we expect a large spot to be smeared out by Keplerian shear. In a time Δt the

azimuthal extent of a hot spot at radius r and radial extent Δr will increase by

$$\frac{\Delta\theta}{2\pi} = \frac{3}{2} \frac{\Delta t}{P} \frac{\Delta r}{r}, \quad (12)$$

where P is the local Keplerian period. Because the hot spot we have considered in our model does not appear to evolve azimuthally over the course of two revolutions (the average value of σ determined for the second cycle of the hot spot, 8° , is no greater than that for the first), it must be very compact ($\Delta r \ll r$). This can be the case if, for example, the hot spot resulted from the oblique impact of a star on the disk, which created a trail of substantial azimuthal extent but small radial extent (note that $r \approx 455 r_g \approx 10^5 M_8 R_\odot$). Alternatively, this may indicate that σ does not measure the actual angular extent of the hot spot, which would presumably be achieved by such a velocity shear, but instead its velocity structure.

The most likely scenarios for a hot spot are those in which there is excess material or energy concentrated in some location with, possibly, some extent in azimuthal angle but little in radius. The most common potential sources of such changes present in an AGN environment are stars (Blandford & Rees 1992), but the exact mechanism is unclear. Stars passing through the disk are expected to remove material, rather than to deposit any, and the material removed should quickly dissipate after it is no longer shielded from the hot, luminous central parts of the disk by an optically thick medium (Zurek, Siemiginowska, & Colgate 1994). Stars should be brought into orbits lying within the disk through the momentum loss that occurs in passages through it; however, due to the concentration of material within the disk, such stars should not then leave its central plane. Therefore, scenarios in which the strong variations in R occur while a star orbits within the disk and subsequently decrease in strength when it begins to leave are untenable.

An alternative scenario is one in which the excess emission comes from a sizable vortex orbiting within the disk (Abramowicz *et al.* 1992). Such a vortex may possess a substantial velocity gradient, explaining the apparent width of the hot spot. However, examination of the power spectrum of the complete set of R values reveals only a single strong peak (with a period corresponding to that measured above) and its aliases; models in which there exists a cascade of large numbers of vortices at many scales predict a power spectrum of roughly power-law form (Abramowicz *et al.* 1991).

It is clear that some type of temporary periodic phenomenon occurs, whatever its origin, and that the most likely way for it to cycle between being blueshifted and redshifted is if it follows an orbit around the central body. The self-consistency of a model in which the hot spot follows a circular orbit is encouraging. The constant angular velocity of the hot spot supports the hypothesis that it is within a circular accretion disk, as independent elliptical orbits do not circularize quickly compared to the orbital period. Thus, a model in which the two peaks of Arp 102B arise in a circular accretion disk seems to be the simplest that can explain the observed phenomena. Even if this model is incorrect, the consistency of the behavior of the variable part of the emission line with a circular orbit suggests that our mass determination should be correct up to an uncertainty in the inclination.

Our measurement of the mass of a possible black hole at the center of Arp 102B is subject to a straightforward test. Unless the hot spot observed was a particularly rare event, other such phenomena should appear in the future and may be subjected to similar analysis. If the spectrum of Arp 102B is observed sufficiently often, an independent mass measurement should result. If our model is correct, those measurements should be consistent, even though a new hot spot may be located at a different radius and have different intensity than the one we observed.

Contrary to previous claims (*e.g.*, Gaskell 1996; Miller & Peterson 1990), the variability of the line profile does not necessarily invalidate the accretion disk hypothesis. Instead, it may provide additional information about the structure and properties of the disk. In the particular case of Arp 102B, the pattern of variability leads to a dynamical measurement of the mass of the central black hole. This method may be applicable to other double-peaked emitters; several have exhibited substantial variation in the blue-to-red flux ratio, for instance, and the variations of their line profiles may not be fitted in detail by the previously posited elliptical accretion disk models. With well-sampled monitoring such as that conducted for 3C 390.3 (Veilleux & Zheng 1991), more mass measurements of this quality might be made.

Most of the data presented in this paper were collected at Kitt Peak National Observatory and Lick Observatory. We are grateful to the members of the staffs for their expert assistance in carrying out the observations, as well as to numerous colleagues who have contributed their efforts to this project. M. E. and J. A. N. acknowledge Hubble Fellowship grant HF-01068.01-94A and a National Science Foundation Fellowship, respectively. This work was also supported by NASA grant G0-06097-94A from the Space Telescope Science Institute (operated by AURA, Inc., under NASA contract NAS5-26555).

REFERENCES

- Abramowicz, M. A., Bao, G., Lanza, A., Zhang, X. H. 1991, *A&A*, 245, 454
Abramowicz, M. A., Lanza, A., Spiegel, E. A., & Szuszkiewicz, E. 1992, *Nature*, 356, 41
Blandford, R. D., & McKee, C. F. 1982, *ApJ*, 255, 419
Blandford, R. D., & Rees, M. J. 1992, in *Testing the AGN Paradigm*, ed. S. S. Holt, S. G. Neff, & C. M. Urry (New York: AIP), 3
Chakrabarti, S., & Wiita, P. J. 1993, *ApJ*, 411, 602
Chakrabarti, S., & Wiita, P. J. 1994, *ApJ*, 434, 518
Chen, K., & Halpern, J. P. 1989, *ApJ*, 344, 115
Chen, K., Halpern, J. P., & Filippenko, A. V. 1989, *ApJ*, 339, 742
Eracleous, M. 1997, *Proc. 31st COSPAR Sci. Assemb., Adv. Sp. Res.*, in press
Eracleous, M., & Halpern, J. P. 1993, *ApJ*, 409, 584

- Eracleous, M., & Halpern, J. P. 1994, *ApJS*, 90, 1
- Eracleous, M., Halpern, J. P., Gilbert, A., Newman, J. A., & Filippenko, A. V. 1997, in preparation
- Eracleous, M., Livio, M., Halpern, J. P., & Storchi-Bergmann, T. 1995, *ApJ*, 438, 610
- Gaskell, C. M. 1983, *Liege Astrophysical Colloq.*, 24, 473
- Gaskell, C. M. 1996, *ApJ*, 464, L107
- Gilbert, A. M., Eracleous, M., Halpern, J. P., & Filippenko, A. V. 1997, in preparation
- Halpern, J. P., Eracleous, M., Filippenko, A. V., & Chen, K. 1996, *ApJ*, 464, 704
- Halpern, J. P., & Filippenko, A. V. 1988, *Nature*, 331, 46
- Halpern, J. P., & Filippenko, A. V. 1992, in *Testing the AGN Paradigm*, ed. S. S. Holt, S. G. Neff, & C. M. Urry (New York: AIP), 59
- Kato, S. 1983, *PASJ*, 35, 249
- Kato, S. 1989, *PASJ*, 41, 745
- Livio, M., & Pringle, J. E. 1996, *MNRAS*, 278, 35L
- Marsh, T. R. 1988, *MNRAS*, 231, 1117
- Marsh, T. R., Horne, K., Schlegel, E. M., Honeycutt, R. K., & Kaitchuck, R. H. 1990, *ApJ*, 364, 637
- Miller, J. S., & Peterson, B. M. 1990, *ApJ*, 361, 98
- Miller, J. S., & Stone, R. P. S. 1987, *Lick Obs. Tech. Rep.*, No. 48
- Miller, J. S., & Stone, R. P. S. 1993, *Lick Obs. Tech. Rep.*, No. 66
- Oke, J. B., & Gunn, J. E. 1982, *PASP*, 94, 586
- Pringle, J. E. 1996, *MNRAS*, 281, 357
- Robinson, L. B., & Wampler, E. J. 1972, *PASP*, 84, 161
- Shakura, N. I., & Sunyaev, R. A. 1973, *A&A*, 24, 337
- Stauffer, J., Schild, R., & Keel, W. 1983, *ApJ*, 270, 465
- Stella, L. 1990, *Nature*, 344, 747
- Storchi-Bergmann, T., Eracleous, M., Ruiz, M.-T., Livio, M., Wilson, A. S., & Filippenko, A. V. 1997, in preparation
- Syer, D., & Clarke, C.J. 1992, *MNRAS*, 255,92
- Veilleux, S., & Zheng, W. 1991, *ApJ*, 377, 89
- Young, P., & Schneider, D. P. 1980, *ApJ*, 238, 955
- Zheng, W., Binette, L., & Sulentic, J.W. 1990, *ApJ*, 365, 115
- Zheng, W., Veilleux, S., & Grandi, S. A. 1991, *ApJ*, 381, 418

Zurek, W. H., Siemiginowska, A., & Colgate, S. A. 1994, *ApJ*, 434, 46

Table 1. Journal of Observations ^a

UT Date	Telescope	Exposure Time (s)	
		H α	H β
1983 Jun 6	Palomar 5 m	b	b
1983 Sep 15	Palomar 5 m	b	b
1985 Jun 28	Palomar 5 m	2500	2500
1986 Jul 13	Lick 3 m	3000	3000
1987 May 4	Lick 3 m	1000	...
1987 Aug 8	Lick 3 m	1300	...
1987 Aug 12	Lick 3 m	1600	...
1989 Apr 27	Lick 3 m	900	...
1989 Jul 1	KPNO 2.1 m	3600	...
1989 Jul 3	KPNO 2.1 m	...	1800
1989 Jul 5	KPNO 2.1 m	835	835
1989 Jul 10	Lick 3 m	900	...
1989 Nov 4	MDM 2.4 m	1800	...
1989 Nov 7	MDM 2.4 m	435	...
1989 Dec 1	Lick 3 m	1600	1600
1990 Feb 23	KPNO 2.1 m	5400	...
1990 Feb 24	KPNO 2.1 m	...	5400
1990 May 30	KPNO 2.1 m	...	2700
1990 Jul 17	Lick 3 m	1800	...
1990 Aug 30	Lick 3 m	1800	...
1990 Nov 11	Lick 3 m	1800	...
1991 Jun 17	KPNO 2.1 m	9790	...
1991 Jun 18	KPNO 2.1 m	1897	...
1991 Jun 19	KPNO 2.1 m	7200	...
1991 Jun 20	KPNO 2.1 m	7200	...
1991 Jul 3	KPNO 2.1 m	7200	...
1991 Jul 4	KPNO 2.1 m	4950	...
1991 Aug 5	Lick 3 m	1500	...
1991 Oct 31	Lick 3 m	1800	...
1992 Apr 21	Lick 3 m	1200	...
1992 May 6	KPNO 2.1 m	7200	7200
1992 May 13	KPNO 2.1 m	...	4800
1992 May 14	KPNO 2.1 m	...	4800

Table 1—Continued

UT Date	Telescope	Exposure Time (s)	
		H α	H β
1992 May 16	KPNO 2.1 m	3600	3600
1992 Aug 3	Lick 3 m	...	1800
1992 Oct 3	Lick 3 m	1800	1800
1992 Nov 19	Lick 3 m	1200	1200
1993 Apr 14	Lick 3 m	900	900
1993 May 16	KPNO 2.1 m	3600	3600
1993 Jun 28	Lick 3 m	900	900
1993 Jul 28	Lick 3 m	2100	2100
1993 Sep 10	Lick 3 m	3000	3000
1993 Sep 25	Lick 3 m	1800	1800
1993 Oct 22	Lick 3 m	1800	1800
1993 Nov 8	Lick 3 m	3000	3000
1994 Apr 18	Lick 3 m	1200	1200
1994 Jun 16	Lick 3 m	2700	2700
1994 Jul 4	KPNO 2.1 m	3600	...
1994 Jul 5	KPNO 2.1 m	3600	...
1994 Jul 15	Lick 3 m	3000	3000
1994 Aug 4	Lick 3 m	3600	3600
1994 Sep 3	Lick 3 m	3600	3600
1994 Oct 1	Lick 3 m	4800	6600
1994 Nov 12	Lick 3 m	3600	2800
1995 Jan 23	KPNO 2.1 m	1800	...
1995 Mar 25	Lick 3 m	1500	1500
1995 Jun 3	KPNO 2.1 m	3600	...
1995 Jun 4	KPNO 2.1 m	3600	3600
1995 Sep 26	Lick 3 m	1800	1800
1996 Feb 13	KPNO 2.1 m	3200	3200
1996 Jun 13	KPNO 2.1 m	1711	1711

^aThe UV Schmidt spectrograph (Miller & Stone 1987) was used for all Lick Observatory observations listed here until the end of 1991; the Kast spectrograph (Miller & Stone 1993) was used thereafter. At Palomar Observatory, we used the Double Spectrograph (Oke & Gunn 1982).

^bThe 1983 Palomar 5 m spectra are composites of several exposures with effective exposure times that are different in different spectral regions

Table 2. Rest Wavelength of Blue Peak

Year	Pogson's Method Å	Gaussian Method Å
1982.43	6451 ^a	...
1985.49	6460.99	6459.02
1986.53	6445.02	6452.96
1987.34	6456.28	6458.06
1987.61	6453.17	6455.81
1989.32	6451.14	6452.61
1989.45	6445.29	6450.93
1989.50	6445.28	6450.93
1989.51	6442.61	6449.56
1989.52	6447.27	6450.58
1989.84	6448.12	6449.97
1989.85	6453.88	6450.37
1989.92	6444.70	6448.28
1990.15	6442.09	6449.17
1990.41	6449.46	6453.35
1990.54	6448.38	6454.19
1990.66	6444.62	6454.06
1990.86	6462.76	6459.21
1991.46	6439.54	6446.19
1991.46	6443.08	6446.01
1991.46	6441.50	6445.80
1991.47	6441.89	6445.86
1991.50	6441.03	6445.77
1991.50	6439.82	6445.07
1991.59	6443.26	6445.31
1991.83	6443.50	6448.06
1992.30	6455.08	6453.72
1992.35	6447.96	6450.49
1992.76	6447.99	6450.99
1992.88	6448.53	6452.70
1993.28	6442.88	6454.19
1993.37	6450.10	6454.42
1993.49	6450.01	6454.43
1993.57	6447.22	6452.24

Table 2—Continued

Year	Pogson’s Method Å	Gaussian Method Å
1993.69	6451.62	6451.42
1993.73	6450.13	6452.09
1993.81	6450.20	6450.74
1993.85	6444.53	6449.09
1994.29	6447.15	6452.81
1994.46	6444.48	6450.06
1994.51	6443.25	6448.78
1994.51	6444.26	6449.56
1994.54	6444.32	6449.47
1994.59	6447.08	6450.97
1994.67	6447.89	6450.77
1994.69	6447.87	6450.77
1994.75	6447.65	6450.94
1994.86	6445.84	6451.48
1995.06	6443.90	6451.27
1995.23	6448.42	6452.15
1995.23	6446.65	6453.84
1995.42	6451.27	6452.71
1995.42	6452.25	6452.58
1995.73	6454.60	6455.81
1996.12	6457.74	6457.55
1996.45	6451.57	6453.34

^aMeasurement was made by eye from the spectrum presented by Stauffer *et al.* (1983).

Table 3. Fitted Model Parameters

UT Date	θ	I	σ	ξ_i	ξ_o	L_{spot}/L_{disk}
1990 Jul 17	...	0	...	305	730	...
1990 Nov 11	115	150	3.0	295	940	0.0065
1991 Jun 18	270	180	8.0	280	940	0.019
1991 Jul 04	270	170	8.0	275	940	0.018
1991 Aug 05	270	150	4.0	305	790	0.010
1991 Oct 31	230	150	19.	240	1000	0.030
1992 May 06	30	190	8.0	280	750	0.023
1992 Oct 03	20	170	5.0	305	770	0.014
1992 Nov 19	28	235	5.0	285	820	0.017
1993 Apr 14	225	140	8.0	320	880	0.019
1993 May 16	185	205	10.	295	820	0.032
1993 Jun 28	196	235	10.	305	900	0.037
1993 Jul 28	220	145	8.0	310	880	0.019
1993 Sep 25	295	160	7.0	320	880	0.019
1993 Oct 22	260	105	9.0	320	880	0.016
1994 Apr 18	175	150	15.	345	650	0.056
1994 Jul 05	140	90	2.5	400	500	0.015
1994 Sep 03	20	115	7.0	350	630	0.021
1994 Oct 01	20	150	5.0	335	700	0.016
1994 Nov 12	45	65	5.0	350	600	0.0092
1995 Jan 23	65	35	5.0	350	650	0.0045
1995 Mar 25	25	70	10.	325	750	0.014
1995 Jun 03	270	20	10.	315	790	0.0035
1996 Jun 13	240	60	4.0	305	790	0.0040

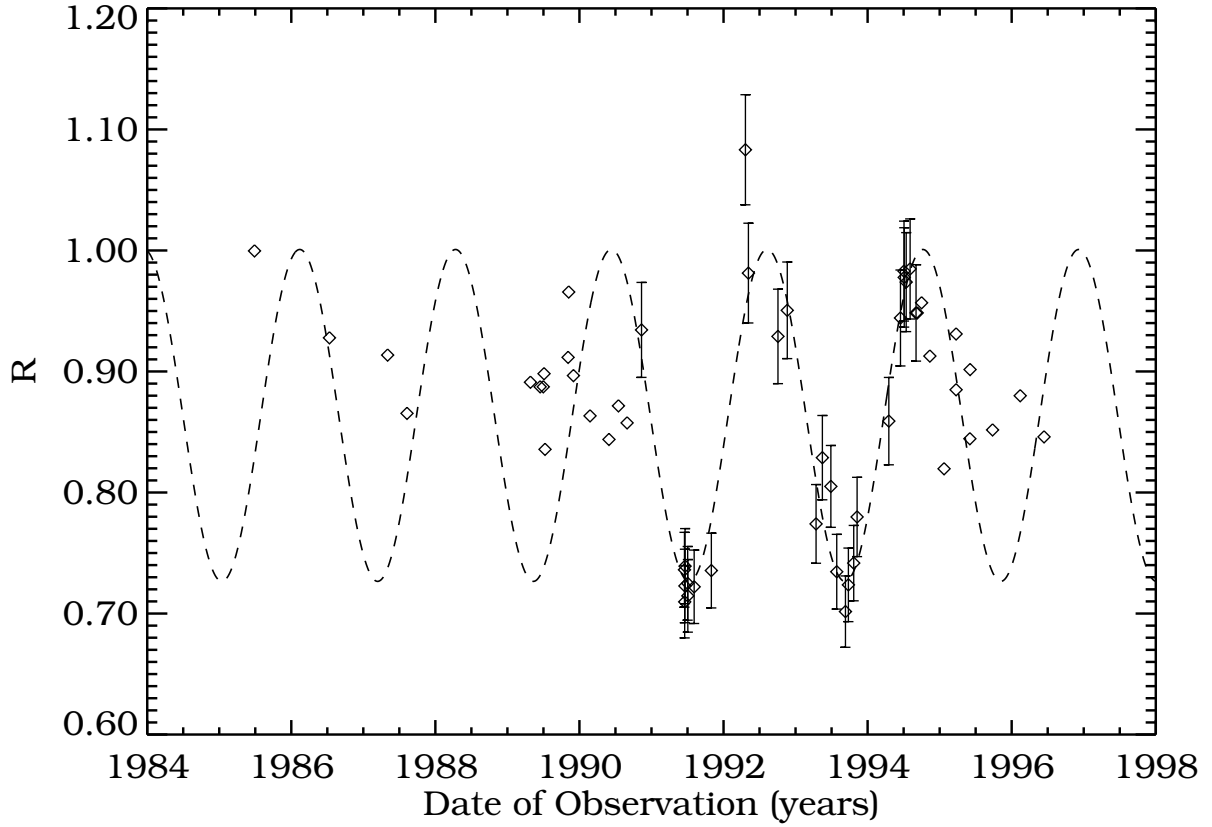


Figure 1 - The evolution of the normalized red-to-blue flux ratio, R , in spectra of Arp 102B. Beginning around November 1990, R varies sinusoidally for several years before returning to its value before the variation began. The sinusoidal curve is a least-squares best fit to those data having error bars shown (corresponding to the epochs from 1990 November 11 through 1994 September 3). Comparison of the residuals for data at similar phases indicates that there is no obvious substantial change in the period of variation during this time.

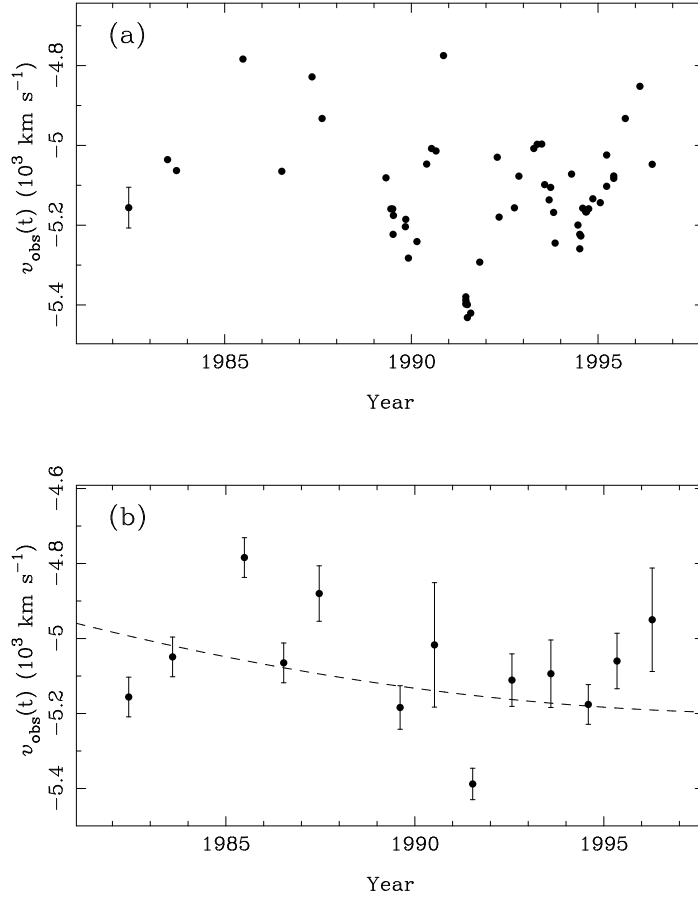


Figure 2. – (a) The variation of the peak velocity of the blue peak as measured from individual spectra using the Gaussian fitting method. A typical error bar of 100 km s^{-1} is shown on the very first point in the sequence for reference. (b) The annually averaged blue peak velocities. The error bars correspond to the dispersion of the velocities measured from individual spectra during that year. The dashed line is the best-fitting sinusoid of equation 4 through these points, which has a period of 390 years and an amplitude of 5200 km s^{-1} .

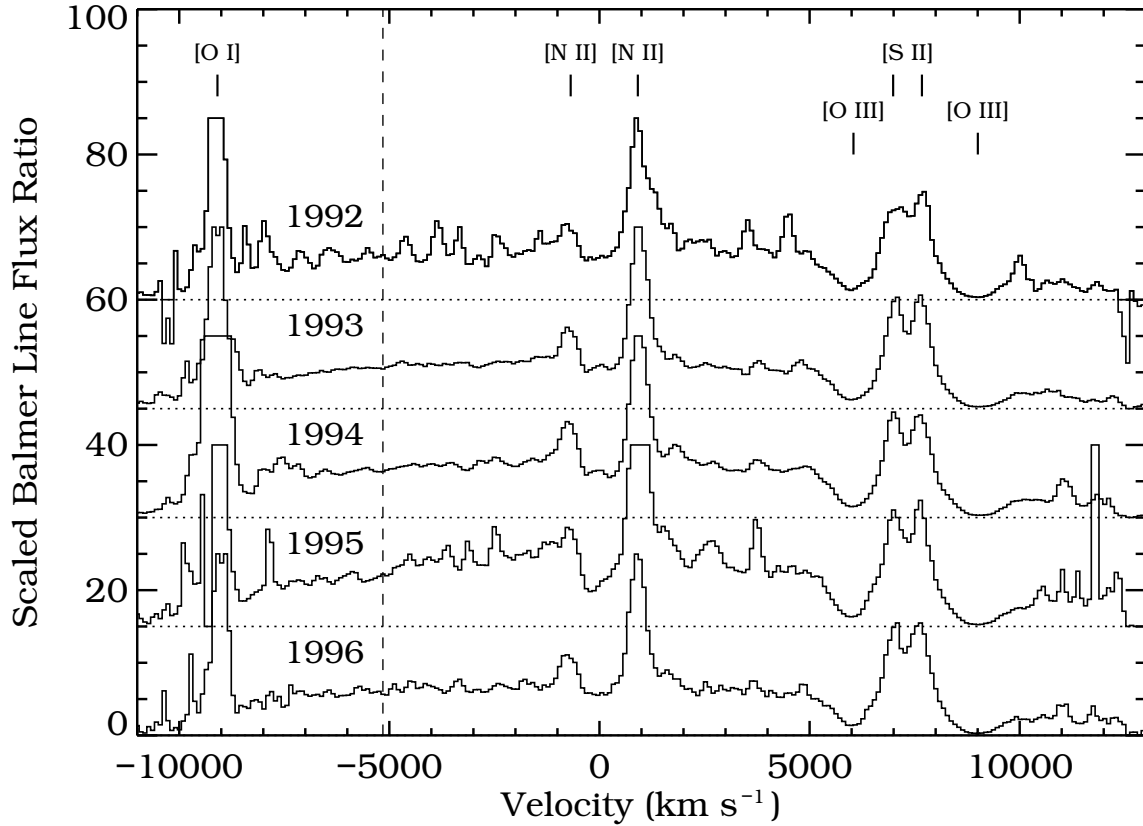


Figure 3 - The rescaled ratios of the annual average of the $H\alpha$ flux for spectra in a given year to the annual average of the $H\beta$ flux in that year. Each average spectrum is indicated by a solid line and is offset by 15 units from spectra of the previous and following years; the zero point for each spectrum is indicated by a dotted line. The dashed line indicates the mean velocity of the blue peak in the $H\alpha$ spectra; all excursions in peak velocity from this value were less than 500 km s^{-1} . The strongest peaks and valleys are associated with the indicated narrow lines near either $H\alpha$ and $H\beta$.

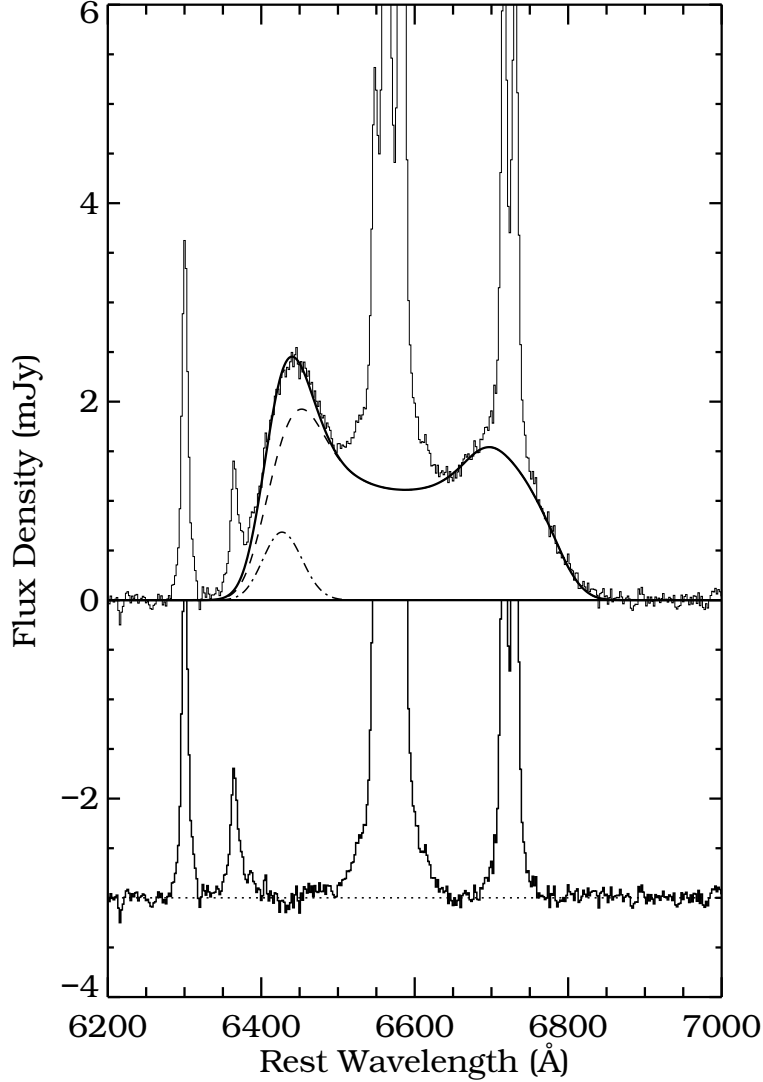


Figure 4 - An example of a fit to a spectrum using our model. The actual spectrum (taken 1991 June 17) and our model fit are indicated with solid curves (some of the narrow emission lines have been truncated in flux density). The dashed line is the flux density in our model fit due to the circular, axisymmetric accretion disk; the dot-dashed line indicates the flux emitted by the hot spot. Finally, the thick solid line indicates the residual when our model fit is subtracted from the actual spectrum, offset by -3 mJy in flux density. Note the resemblance of this residual to the spectrum of a typical broad-line radio galaxy. The model parameters of the fit are $\xi_i=280$, $\xi_o=940$, $\xi_{hot}=455$, $\theta = 270^\circ$, $I=180$, and $\sigma = 8^\circ$.

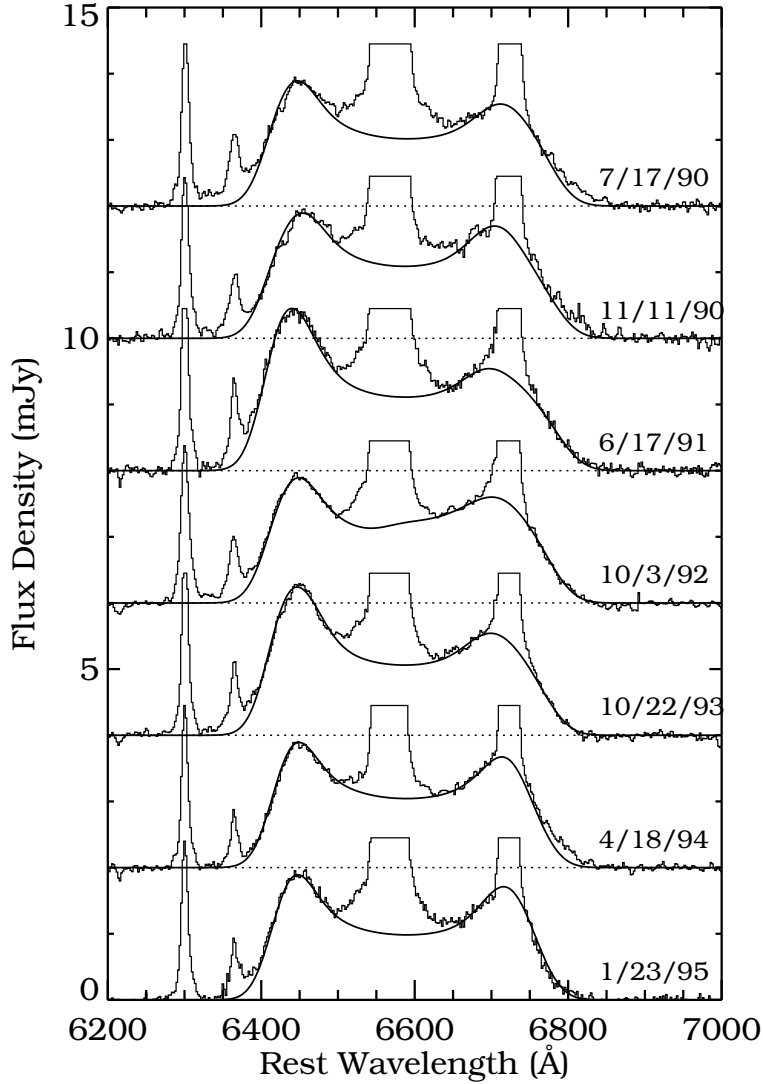


Figure 5 - A set of spectra representative of the evolution of Arp 102B. Spectra are separated by arbitrarily adding a multiple of 2 mJy; the zero point for each spectrum is indicated by a dotted line. The first spectrum, from 1990 July 17, includes no hot spot component. However, the spectra from 1990 November 11 through 1995 January 23 include a hot spot at an azimuth angle of 115, 270, 160, 280, 5, and 115 degrees, respectively, corresponding to hot spots centered at roughly 6842, 6255, 6668, 6260, 6590, and 6842 Å. Substantially different spectra are all fitted by the model. The amplitude of the hot spot had begun to decrease by 1995.

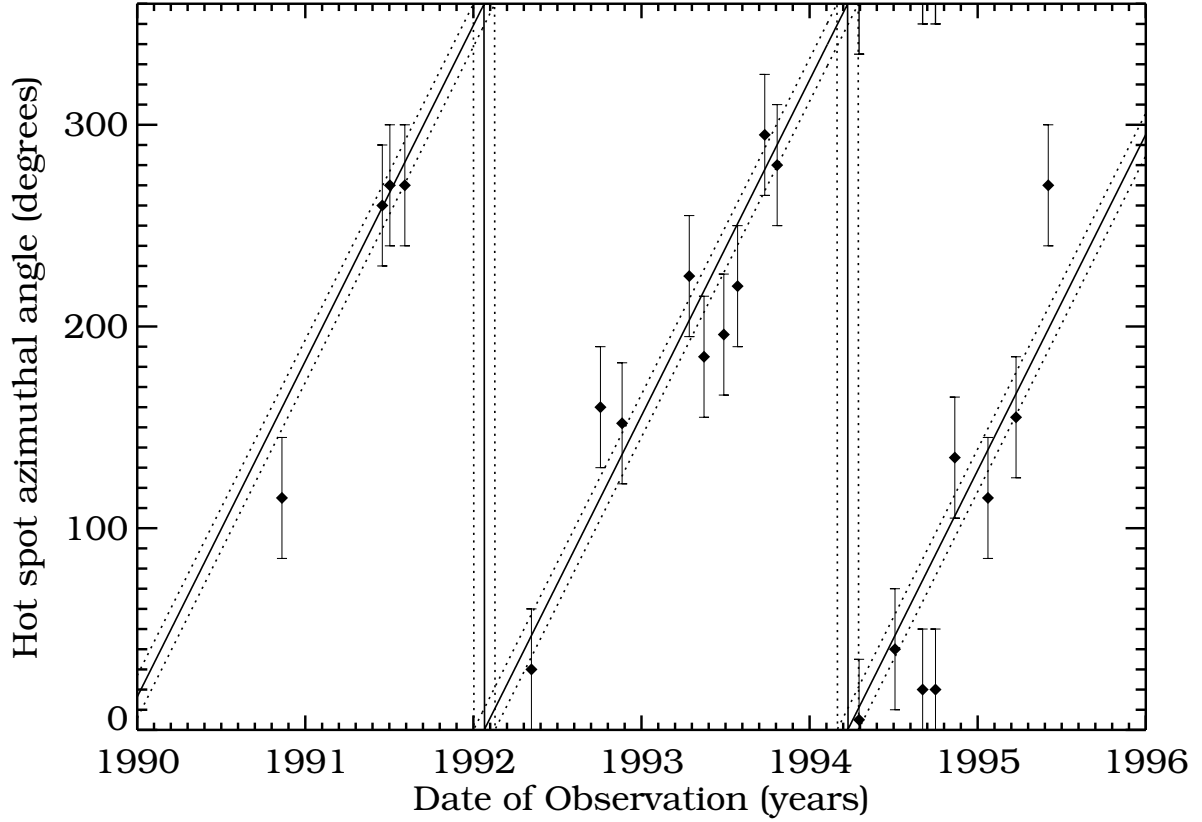


Figure 6 - The azimuthal angle of the hot spot measured from our model fits. The solid line is not a fit to the data shown here, but instead is the increasing phase angle of the sinusoid fit shown in Figure 1; the dotted lines indicate the 1σ error bounds of that fit. At each epoch, there are two possible values of the azimuthal angle due to degeneracies in our model; the possible angle which lies closest to the line is plotted here. Note that there is no systematic pattern in the scatter of data about the line from different epochs with similar phase. It is thus unlikely that the angular velocity varies substantially but periodically (as would be expected for an object on an elliptical orbit).